Approximate relation between black hole perturbation theory and numerical relativity

Tousif Islam[1,2,3,*] and Gaurav Khanna[4,1,3]

[1]*Department of Physics, University of Massachusetts, Dartmouth, Massachusetts 02747, USA*
[2]*Department of Mathematics, University of Massachusetts, Dartmouth, Massachusetts 02747, USA*
[3]*Center for Scientific Computing and Data Science Research, University of Massachusetts, Dartmouth, Massachusetts 02747, USA*
[4]*Department of Physics and Center for Computational Research, University of Rhode Island, Kingston, Rhode Island 02881, USA*

(Received 19 July 2023; accepted 16 November 2023; published 19 December 2023)

We investigate the interplay between numerical relativity (NR) and adiabatic point-particle black hole perturbation theory (ppBHPT) in the comparable mass regime for quasicircular nonspinning binary black holes. Specifically, we reassess the α-β scaling technique, previously introduced by Islam *et al.* [Surrogate model for gravitational wave signals from nonspinning, comparable-to large-mass-ratio black hole binaries built on black hole perturbation theory waveforms calibrated to numerical relativity, Phys. Rev. D **106**, 104025 (2022)], as a means to effectively match ppBHPT waveforms to NR waveforms within this regime. In particular, α rescales the amplitude and β rescales the time (and hence the phase). Utilizing publicly available long NR data (`SXS:BBH:2265` [SXS Collaboration, Binary black-hole simulation `SXS:BBH:2265` (2019)]) for a mass ratio of 1:3, encompassing the final ∼65 orbital cycles of the binary evolution, we examine the range of applicability of such scalings. We observe that the scaling technique remains effective even during the earlier stages of the inspiral. Additionally, we provide commentary on the temporal evolution of the α and β parameters and discuss whether they can be approximated as constant values. Consequently, we derive the α-β scaling as a function of orbital frequencies and demonstrate that it is equivalent to a frequency-dependent correction. We further provide a brief comparison between post-Newtonian (PN) waveforms and the rescaled ppBHPT waveform at a mass ratio of 1:3 and comment on their regime of validity. Finally, we explore the possibility of using PN theory to obtain the α-β calibration parameters and still provide a rescaled ppBHPT waveform that matches NR.

DOI: 10.1103/PhysRevD.108.124046

I. INTRODUCTION

Development of computationally efficient yet precise waveform models [1–15] binary black hole (BBH) mergers play a crucial role in GW research. This relies heavily on accurate numerical simulations of BBH mergers. In the regime of comparable mass ratios ($1 \leq q \leq 10$ where $q \coloneqq m_1/m_2$ represents the mass ratio of the binary, with m_1 and m_2 denoting the masses of the primary/larger and secondary/smaller black holes, respectively), the most accurate approach to simulate a BBH merger is by solving the Einstein equations using numerical relativity (NR) [16–23] (Fig. 1). However, accurately simulating BBH mergers using NR in the intermediate- to large-mass ratio regime ($10 \leq q \leq 100$) remains a challenging task due to algorithmic complexity.

In contrast, adiabatic point-particle black hole perturbation theory (ppBHPT) [24–33] offers a reliable modeling approach for extreme mass ratio inspirals (EMRI) ($q \to \infty$) (Fig. 1). In ppBHPT, the smaller black hole is treated as a point particle orbiting the larger black hole described by a curved space-time background. However, as the binary system becomes less asymmetric and approaches the regime of comparable mass ratios, the assumptions of the ppBHPT framework begin to break down. Consequently, the ppBHPT framework fails to generate accurate gravitational waveforms within this regime. On the other hand, post-Newtonian (PN) theories [34] provide a dependable approximate method to generate gravitational waveforms for BBH mergers during the inspiral stage of the binary evolution when the two black holes are considerably distant from each other and their velocities are significantly smaller than the speed of light (Fig. 1).

In recent times, there have been significant advancements in expanding the scope of both NR and ppBHPT frameworks. These advancements include the development of the `BHPTNRSur1dq1e4` surrogate model [35,36], a fully relativistic second-order self-force model [37], and the extension of NR techniques to simulate BBH mergers with higher-mass ratios [38–41].

*tislam@umassd.edu

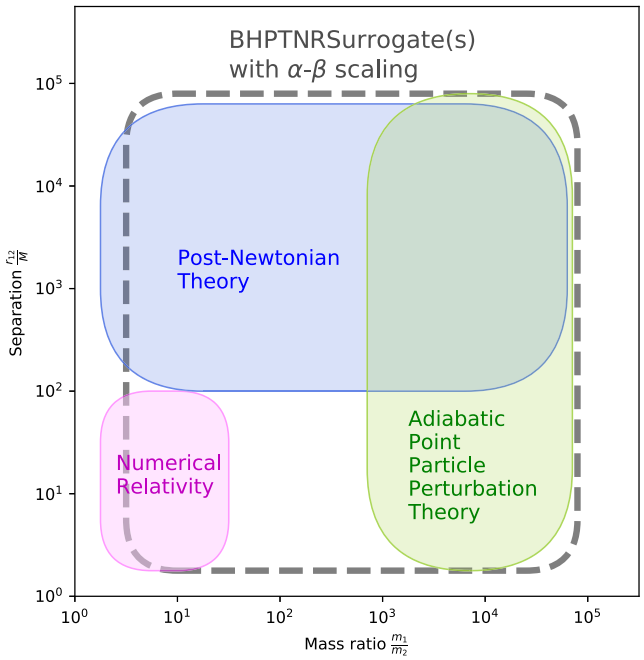

FIG. 1. We show the approximate schematic of the regime of validity of three different methods to simulate BBH mergers; NR, ppBHPT, and post-Newtonian approximations. For comparison, we show the regime of validity of the NR-tuned ppBHPT surrogate models [named collectively as `BHPTNRSurrogate(s)`] that employs a rescaling technique called α-β scaling to match ppBHPT waveforms to NR in the comparable mass regime. Here, x-axis shows the mass ratio $\frac{m_1}{m_2}$ whereas y-axis shows the separation r_{12} (scaled by the total mass of the binary $M \coloneqq m_1 + m_2$) between the two component black holes in a binary. More details are in Sec. I.

The `BHPTNRSur1dq1e4` surrogate model, which relies on the ppBHPT framework, has exhibited reasonable accuracy in predicting waveforms for BBH mergers in the comparable to large mass ratios regime. By employing a straightforward calibration procedure known as the α-β scaling, the ppBHPT waveforms are appropriately rescaled to achieve excellent match with NR data, particularly in the comparable mass regime. The scaling reads [36]

$$h^{\ell,m}_{\rm NR}(t_{\rm NR};q) \sim \alpha_\ell h^{\ell,m}_{\rm ppBHPT}(\beta t_{\rm ppBHPT};q), \tag{1}$$

where $h^{\ell,m}_{\rm NR}$ and $h^{\ell,m}_{\rm ppBHPT}$ represent the NR and ppBHPT waveforms, respectively, as functions of the NR time $t_{\rm NR}$ and ppBHPT time $t_{\rm ppBHPT}$. The calibration parameters, α_ℓ and β, are typically determined through matching ppBHPT waveforms to NR. Following the α-β calibration procedure, the quadrupolar mode of the rescaled ppBHPT waveform exhibits an excellent agreement with NR, with errors of approximately 10^{-3} or less, in the comparable mass regime [36]. Additionally, the rescaled ppBHPT waveforms demonstrate a remarkable match to recently obtained NR data in the high-mass ratio regime ($q = 15$ to $q = 128$) [42]. It has been shown that these waveforms can be used to accurately estimate the properties of the final black holes [43]. Further analysis provides evidence that the calibration parameters can be attributed to the absence of finite-size effects within the ppBHPT framework [44].

In this paper, we investigate the interplay between NR and ppBHPT in the comparable mass regime through the lens of the α-β scaling. In particular, we use publicly available long NR data (`SXS:BBH:2265`), for a mass ratio of $q = 3$, that covers the final ∼65 orbital cycles of the binary evolution to understand applicability of the α-β scaling. This particular NR data is almost ten times longer in duration than most of the existing NR data and have significantly more cycles. In Sec. II, we present our main findings and results. To begin, Sec. II A explores different methods to obtain the calibration parameters α and β. Next, in Sec. II B, we provide a detailed comparison of the α and β values obtained from these different approaches. Section II C then comments on the regime of validity of the α-β scaling. Finally, in Sec. IV, we discuss the implication of our results in current and future efforts in modeling gravitational waveforms from BBH mergers.

II. SCALING BETWEEN NR AND PERTURBATION THEORY

In this section, we present a detailed analysis of the α-β scaling between ppBHPT and NR waveforms in the comparable mass regime. To do this, we utilize publicly available long NR data (`SXS:BBH:2265` [45]), for a mass ratio of $q = 3$. The NR data covers the final ∼65 orbital cycles of the binary evolution and are $\sim 30000M$ long in duration (where M is the total mass of the binary). We then generate the ppBHPT waveform for this mass ratio using the framework developed in Refs. [24–27]. In particular, we first compute the full inspiral-merger-ringdown trajectory taken by the point particle and then we use that trajectory to compute the gravitational wave emission by solving the inhomogeneous Teukolsky equation in the time domain [24–27,46]. A brief summary of our framework is given in Sec. II of Ref. [36]. Our ppBHPT waveform data covers the final ∼56 orbital cycles of the binary evolution and are $\sim 35000 m_1$ long in duration.

A. Methods to obtain α-β values

Once we have both the ppBHPT and NR data for $q = 3$, we investigate various methods to determine the appropriate α_ℓ and β values necessary for accurately rescaling the ppBHPT waveform to achieve a strong agreement with NR. To simplify the analysis, we focus on the (2, 2) mode of the waveform. Subsequently, we drop the subscript ℓ and use only α unless otherwise mentioned.

1. Using full waveform data

Typically, the values of α and β are determined by minimizing the L_2-norm difference between the NR data

and the rescaled ppBHPT waveforms, covering full inspiral-merger-ringdown stage of the binary evolution, after aligning them on the same time grid [35,36]. The optimization problem can be formulated as follows:

$$\min_{\alpha,\beta} \frac{\int |\alpha h^{2,2}_{\rm ppBHPT}(\beta t_{\rm ppBHPT}) - h^{2,2}_{\rm NR}(t_{\rm NR})|^2 dt}{\int |h^{2,2}_{\rm NR}(t_{\rm NR})|^2 dt}. \quad (2)$$

This optimization problem yields the global best-fit values of α and β that minimize the error computed over the entire length of the waveform data or the calibration regime (e.g., $t \in [-5000, 100]M$ as used in [36]).

2. Using only inspiral data

We can modify the procedure described in Sec. II A 1 by limiting the global fit to only include inspiral data, such as data up to $t = -100M$. This approach eliminates the influence of the merger-ringdown portion of the waveform, which may have different mass scale and spin values.

3. Using the peaks

Alternatively, it is possible to estimate the optimal values of α and β at different points during the binary evolution. However, special care should be taken as this approach requires simultaneous rescaling of both the time and amplitude.

We note that, in order to achieve a successful rescaling, it is necessary for the peaks of the waveform to align between the NR and ppBHPT data for a given cycle before merger. Therefore, we can estimate the optimal values of α and β at each peak by matching the peak time and value between NR and ppBHPT. For instance, we can focus on the 50th peak before the merger in both NR and ppBHPT waveforms. By employing cubic splines, we can accurately determine the precise location and value of the peak from the discrete waveform data in both cases. Let us denote the peak times as $t_{\rm peak,ppBHPT}$ and $t_{\rm peak,NR}$, while the peak values are denoted as $h_{\rm peak,ppBHPT}$ and $h_{\rm peak,NR}$. In this analysis, the point estimates of α and β at the peaks are given by

$$\alpha_{\rm peak} = \frac{h_{\rm peak,NR}}{h_{\rm peak,ppBHPT}}, \quad (3)$$

and

$$\beta_{\rm peak} = \frac{t_{\rm peak,NR}}{t_{\rm peak,ppBHPT}}. \quad (4)$$

By repeating this analysis for all the peaks, we can obtain a temporal variation of the optimal local values of α and β throughout the binary evolution.

4. Using a certain number of cycles

Finally, we can modify the method to estimate the local values of α and β throughout the binary evolution by considering a broader time window instead of just focusing on individual peaks. For example, we can choose to match the ppBHPT and NR waveforms between the 50th and 41st peak before the merger. The shorter duration NR and ppBHPT data, which are restricted to the selected time window, can be denoted as $(t^{\rm NR}{\rm win}, h^{\rm NR}{\rm win})$ and $(t^{\rm ppBHPT}{\rm win}, h^{\rm ppBHPT}{\rm win})$, respectively. We then perform the α-β scaling as described in Eq. (1) on these dataset by minimizing the following difference:

$$\min_{\alpha,\beta} \frac{\int |\alpha h^{\rm win}_{\rm ppBHPT}(\beta t^{\rm win}_{\rm ppBHPT}) - h^{\rm win}_{\rm NR}(t^{\rm win}_{\rm NR})|^2 dt}{\int |h^{\rm win}_{\rm NR}(t^{\rm win}_{\rm NR})|^2 dt}. \quad (5)$$

This minimization problem yields the global best-fit values of α and β that minimize the error computed over the entire length of the waveform data or the calibration regime (e.g., $t \in [-5000, 100]M$ as used in [36]).

This approach allows us to obtain an averaged local estimate of the α and β values around the time corresponding to the mean of the time window between the 50th and 41st peak before the merger. In this modified approach, we utilize 10 cycles of waveform data to estimate the α and β values, which we denote as $\alpha_{\rm 5cycles}$ and $\beta_{\rm 5cycles}$.

B. Comparison of the α-β values from different methods

To infer both global and local estimates of the α and β values for $q = 3$, we first employ three different techniques:

(i) We use the final $\sim 5000M$ of the NR data to find the global best-fit values of α and β. This is done by minimizing the L_2-norm difference between the rescaled ppBHPT waveform and the NR waveform, as described in Sec. II A 1. The obtained calibration values are denoted as α_{5000M} and β_{5000M}.

(ii) We match all 112 peaks in the NR data to their corresponding peaks in the ppBHPT waveform using the procedure outlined in Sec. II A 3. This gives us the point estimates of α and β at each peak, denoted as $\alpha_{\rm peak}$ and $\beta_{\rm peak}$.

(iii) The NR data is divided into smaller windows consisting of 10 consecutive peaks (i.e. 5 cycles), resulting in 10 smaller time windows. We then apply the procedure described in Sec. II A 4 to match each of these smaller windows to the corresponding ppBHPT waveforms. This provides us with the averaged local estimations of the calibration parameters, denoted as $\alpha_{\rm 5cycles}$ and $\beta_{\rm 5cycles}$.

By employing these three techniques, we can obtain a comprehensive understanding of the α and β values for the considered mass ratio of $q = 3$.

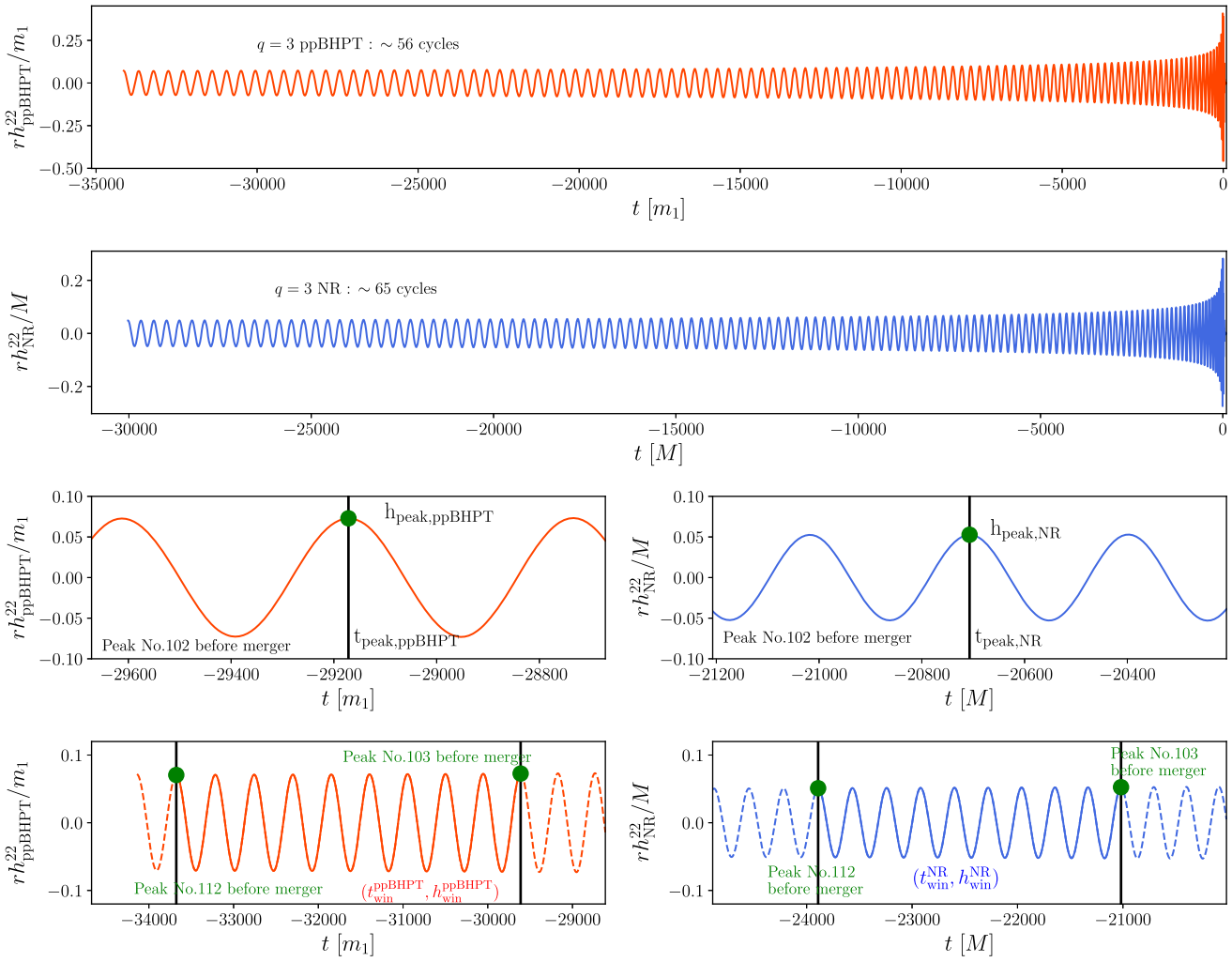

FIG. 2. Comparison of the (2, 2) mode of the NR (first row) and ppBHPT (second row) waveforms for $q = 3$, along with the 102nd peak of both waveforms (third row) and the waveform segment between the 102nd and 103rd peaks (fourth row). This visualization demonstrates the waveform portion used in different approaches to estimate the α and β values. More details are in Sec. II B.

Figure 2 illustrates the (2, 2) mode of the NR (first row) and ppBHPT waveforms (second row), both aligned such that the maximum amplitude occurs at $t = 0$ and the orbital phase is zero at the beginning. This alignment facilitates a direct comparison between the two waveforms. Additionally, we highlight the 102nd peak of both waveforms (third row), along with their corresponding peak times. It is evident that the peak times and values differ between the NR and ppBHPT waveforms due to dephasing between the NR and adiabatic approximation of the ppBHPT. The peaks in the ppBHPT waveform occur earlier in time and have larger amplitudes compared to the NR waveform. This emphasizes the need to establish a scaling relationship between the ppBHPT and NR waveforms. Finally, we show the waveform segment between the 102nd and 103rd peaks for both NR and ppBHPT as a demonstration of the procedure mentioned in Sec. II A 4.

In Fig. 3, we compare the obtained values of α and β from different approaches. We observe that $\alpha_{\rm peak}$ remains relatively constant throughout the binary evolution, while $\beta_{\rm peak}$ shows stability in the earlier stages and deviates slightly during the late-inspiral-merger phase. It is important to note that $\alpha_{\rm peak}$ and $\beta_{\rm peak}$ represent local optimal values and may differ slightly from the global fit values, e.g., α_{5000M} and β_{5000M}. We also examine $\alpha_{\rm 5cycles}$ and $\beta_{\rm 5cycles}$, which provide averaged local estimations of the calibration parameters. We note that $\alpha_{\rm 5cycles}$ closely follows $\alpha_{\rm peak}$, while $\beta_{\rm 5cycles}$ aligns well with $\beta_{\rm peak}$, except for the late-inspiral and merger region where some deviations occur for β. We further note that the obtained values of α and β from the different approaches are not simply consistent with the naive mass-scale transformation of $\frac{1}{1+1/q}$. This naive mass-scale transformation is required to transform the mass-scale of the ppBHPT waveforms from m_1 to M. This suggests that the calibration parameters α and β encompass additional effects beyond a simple mass-scale transformation. Next, we plot the α and β from

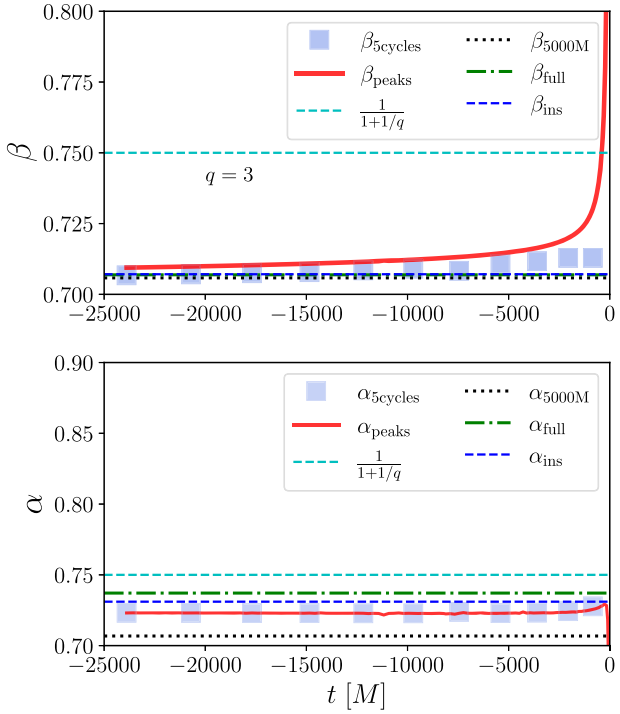

FIG. 3. We show the α and β values for $q = 3$ obtained from different approaches outlined in Sec. II A. For comparison, we also show the naive scaling of $\frac{1}{1+1/q}$ required to ensure consistency in mass scale between ppBHPT and NR. More details are in Sec. II B.

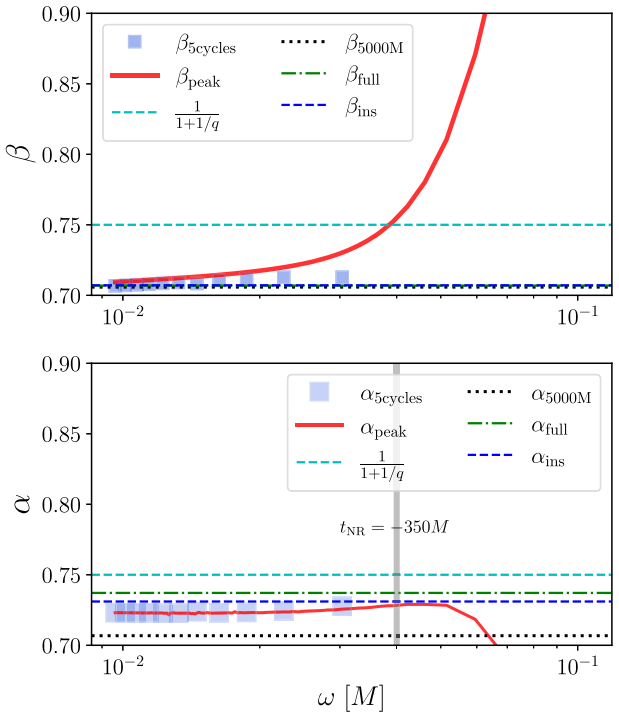

FIG. 4. We show the α and β values for $q = 3$ obtained from different approaches as a function of the NR orbital frequencies. For comparison, we also show the naive scaling of $\frac{1}{1+1/q}$ required to ensure consistency in mass scale between ppBHPT and NR. More details are in Sec. II B.

different approaches as a function of the NR orbital frequencies (Fig. 4). This further demonstrates that the α and β values are mostly constant for a significant portion of the frequency window.

In Fig. 5, we therefore investigate the applicability of the α-β scaling to the entire length of the available NR data by utilizing the full $30000M$ of NR waveform data, covering 56 cycles, along with the corresponding $\sim 35000 m_1$ ppBHPT waveform data. By employing Eq. (1) and following the procedure outlined in Sec. II A 1, we successfully obtain a set of α and β values that allow us to rescale the full ppBHPT waveform to match the NR data throughout the binary evolution. Note that these values are denoted as α_{full} and β_{full} and are also shown in Figs. 3 and 4 for comparison. In the top row of Fig. 5, we show the NR data and the ppBHPT waveforms after applying the scaling factor of $\frac{1}{1+1/q}$. Additionally, we present the rescaled ppBHPT waveform after the α-β calibration in the second row. In the third row of Fig. 5, we show $\Delta A/A_{\text{NR}}$, relative error in amplitude, and $\Delta\phi_{\text{NR}}$, absolute error in the phase, of both the ppBHPT (after multiplying the waveform with the factor $\frac{1}{1+1/q}$ to have the same mass scale of NR) and rescaled ppBHPT waveform when compared to the NR data. These errors indicate that the rescaled ppBHPT waveform exhibits excellent agreement with the NR data, with amplitude errors on the order of $\sim 0.1\%$ and phase errors of approximately ~ 0.1 radians. These errors are significantly smaller compared to the errors between the original ppBHPT waveform (after multiplying the factor of $\frac{1}{1+1/q}$) and the NR data, demonstrating the effectiveness of the α-β scaling in improving the agreement between the two waveforms.

Finally, to understand and mitigate the effect of the merger-ringdown waveform in the α-β calibration, we follow the procedure outlined in Sec. II A 2 and use only the waveform up to $t = -100M$. The resulting calibration parameters are denoted as α_{ins} and β_{ins}. We find that α_{ins} and β_{ins} are very close to α_{full} and β_{full}, respectively. Specifically, we have

$$[\alpha_{\text{full}}, \beta_{\text{full}}] = [0.737122, 0.706900]$$

and

$$[\alpha_{\text{ins}}, \beta_{\text{ins}}] = [0.731040, 0.707100].$$

We show the values in Figs. 3 and 4 for comparison. These values suggest that the inspiral-only waveform has a slightly larger effect on the α value compared to the β value. However, since the values are very close, it implies that we can use any segment of the waveform and still

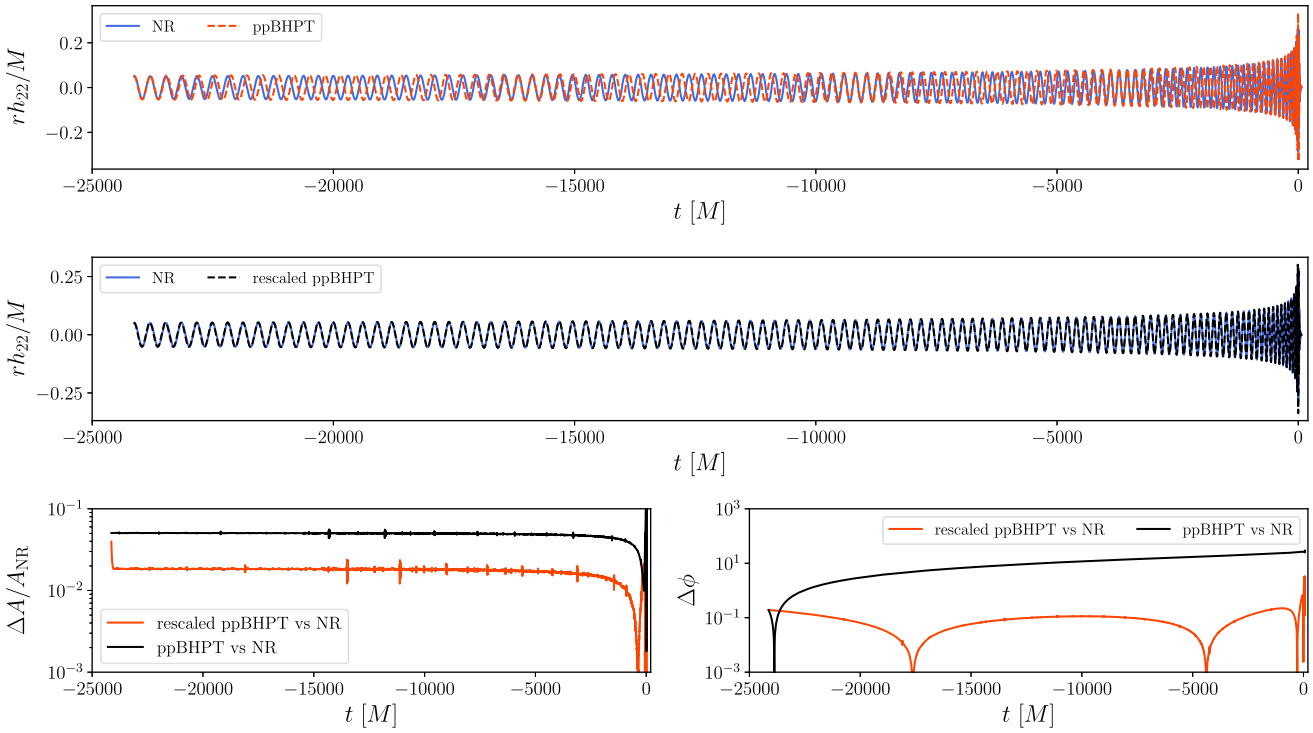

FIG. 5. We show the comparison of the (2, 2) mode of the NR and ppBHPT waveforms (first row), along with the comparison between NR and rescaled ppBHPT waveforms (second row) for $q = 3$. Additionally, we show the errors in the amplitudes and phases (third rows) for both the waveforms when compared to NR. All waveforms have the mass scale of M. More details are in Sec. II B.

obtain meaningful estimates for the α and β parameters. We will demonstrate this later in Sec. III B (cf. Figs. 10 and 11).

C. Validity of the α-β scaling

The results presented in Sec. II B provide valuable insights into the validity and behavior of the α-β scaling between ppBHPT waveforms and NR data for $q = 3$. This insight provides a reasonable understanding into the validity of the scaling in the comparable mass regime. The key findings are as follows:

(i) The scaling procedure is effective even for longer NR simulations with a duration of approximately $30000M$. This demonstrates that the α-β scaling can be successfully applied to a wide range of waveform data, including those with a significant number of orbital cycles.

(ii) Throughout most of the binary evolution, the optimal values of α and β remain approximately constant. This indicates that a global set of calibration parameters can reasonably capture the local behavior.

(iii) In the late-inspiral and merger stage, slight deviations from constant values are observed for both α and β. As a result, the scaling remains extremely effective until very close to merger (up to $\sim 40M$ before the merger) beyond which slight differences between rescaled ppBHPT and NR is observed. We can attribute these deviations to the changes in mass and spin of the final black hole during this phase. Reference [43] has shown that the α and β values, obtained in the inspiral part of the waveform, can be self-consistently rescaled for the merger-ringdown part using the energy and angular momenta changes up to plunge. In particular, the $\alpha_{\rm MR}$ and $\beta_{\rm MR}$, calibration parameters to match ppBHPT waveform to NR at the merger-ringdown part, obeys the following scaling with $\alpha_{\rm full}$ and $\beta_{\rm full}$ [43]:

$$\alpha_{\rm MR} = \xi \times \alpha_{\rm full}, \tag{6}$$

and

$$\beta_{\rm MR} = \frac{\beta_{\rm full}}{\xi}, \tag{7}$$

where the scaling factor can be approximated as $\xi = [1 - (\frac{\Delta J^z}{M^2})^{1.5}](1 - \frac{\Delta E}{M})$. Here, ΔE and ΔJ^z are the change in energy and angular momentum up to the plunge. Additionally, $\alpha_{\rm MR}$ and $\beta_{\rm MR}$ are the scaling parameters at the merger-ringdown part.

Overall, these findings support the applicability and robustness of the α-β scaling approach in relating ppBHPT waveforms to NR data in the comparable mass regime.

D. Understanding α-β scaling as frequency-dependent corrections

The α-β scaling between ppBHPT and NR waveforms is designed to address the missing finite-size effects [44] and higher-order self-force corrections [37] in ppBHPT waveforms. Wardell *et al.* [37] have shown that the second-order self-force correction (as well as the leading-order term) is frequency dependent. It raises the question of how the α-β scaling can handle frequency-dependent corrections. We now therefore derive the α-β scaling as a function of the orbital frequencies and show explicitly that α-β scaling introduces frequency dependent corrections.

The α-β scaling for the (2, 2) mode can be expressed as follows:

$$h^{2,2}_{\rm NR}(t_{\rm NR};q) \sim \alpha h^{2,2}_{\rm ppBHPT}(\beta \times t_{\rm ppBHPT};q). \tag{8}$$

This scaling relationship extends to the amplitude and phase of the waveforms,

$$A^{2,2}_{\rm NR}(t_{\rm NR}) \approx \alpha \times A^{2,2}_{\rm ppBHPT}(\beta \times t_{\rm ppBHPT}), \tag{9}$$

and

$$\phi^{2,2}_{\rm NR}(t_{\rm NR}) \approx \phi^{2,2}_{\rm ppBHPT}(\beta \times t_{\rm ppBHPT}). \tag{10}$$

One can compute the orbital phase as

$$\begin{aligned} \phi_{\rm orb,NR} &= \phi^{2,2}_{\rm NR}/2, \\ \phi_{\rm orb,ppBHPT} &= \phi^{2,2}_{\rm ppBHPT}/2. \end{aligned} \tag{11}$$

This leads to

$$\frac{d\phi_{\rm orb,NR}}{dt_{\rm NR}} \approx \frac{d\phi_{\rm orb,ppBHPT}}{d(t_{\rm ppBHPT})}\frac{dt_{\rm ppBHPT}}{dt_{\rm NR}}. \tag{12}$$

Simplifying further, we find

$$\omega_{\rm orb,NR} \approx \omega_{\rm orb,ppBHPT}\frac{dt_{\rm ppBHPT}}{dt_{\rm NR}}, \tag{13}$$

where $\omega_{\rm NR}$ and $\omega_{\rm ppBHPT}$ are the orbital frequencies of the NR and ppBHPT waveforms respectively. Since $t_{\rm NR} = \beta t_{\rm ppBHPT}$, we can further simplify it as

$$\omega_{\rm orb,NR} \approx \omega_{\rm orb,ppBHPT} \times \frac{1}{\beta}. \tag{14}$$

Thus, the α-β scaling relationship between ppBHPT and NR waveforms (where both of them are expressed as a function of time), given in Eq. (8), can be equivalently

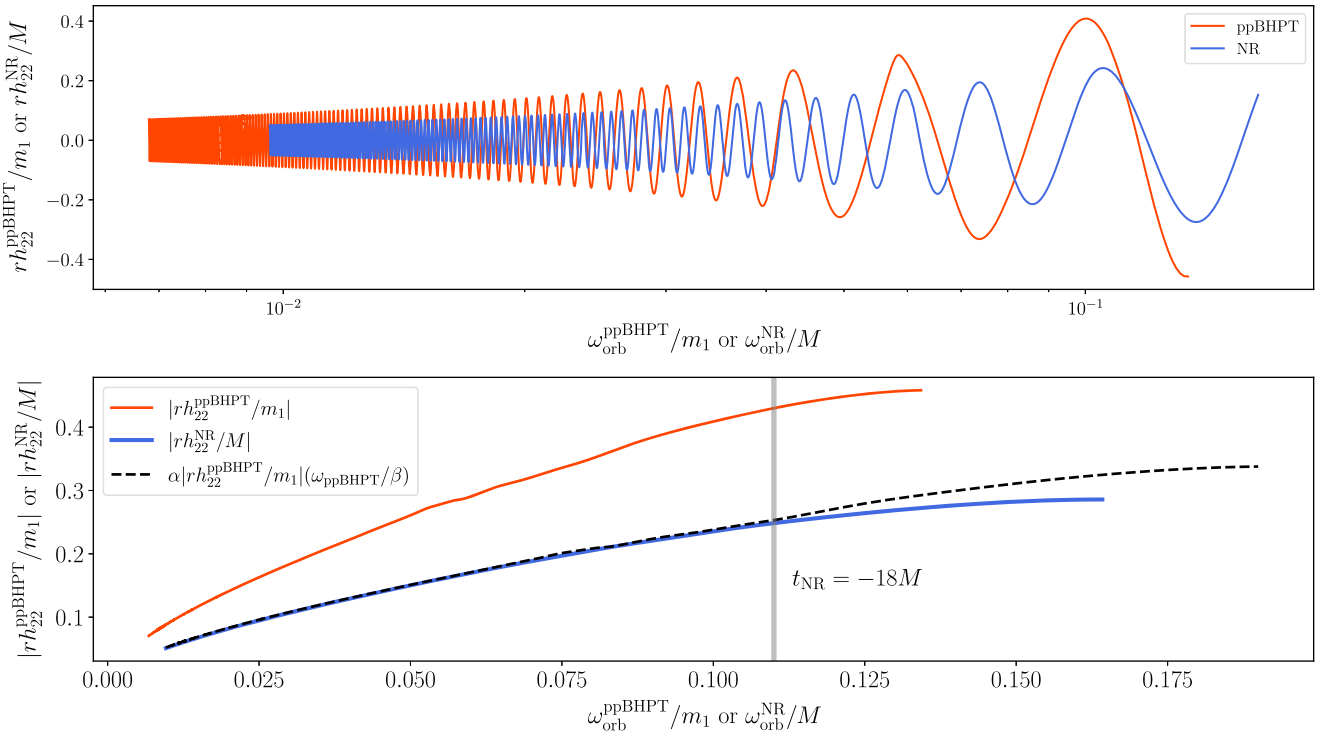

FIG. 6. We show the (2, 2) mode of the NR and ppBHPT waveforms, up to the merger i.e., $t = 0$, as a function of the orbital frequencies, using the mass-scale of M for NR and m_1 for ppBHPT (upper panel) for $q = 3$. The lower panel shows the amplitudes of the waveforms as a function of the orbital frequencies. For comparison, we also show the amplitudes obtained using the approximate scaling in Eq. (17) (lower panel). The gray vertical line represents the time $t_{\rm NR} = -18M$ up to which the scaling works really well. More details are in Sec. II D.

expressed as a scaling between the waveforms as a function of the orbital frequencies. These scalings are

$$A^{2,2}_{\rm NR}(\omega_{\rm orb,NR}) \approx \alpha \times A^{2,2}_{\rm ppBHPT}\left(\frac{\omega_{\rm orb,ppBHPT}}{\beta}\right), \quad (15)$$

and

$$h^{2,2}_{\rm NR}(\omega_{\rm orb,NR}) \approx \alpha \times h^{2,2}_{\rm ppBHPT}\left(\frac{\omega_{\rm orb,ppBHPT}}{\beta}\right). \quad (16)$$

In Fig. 6, we present the (2, 2) mode of the NR and ppBHPT waveforms up to merger as a function of the orbital frequencies in the upper panel, accompanied by the amplitudes in the lower panel. It is evident that any rescaling aiming to match the ppBHPT amplitude (plotted against orbital frequencies; red solid line) to NR (also against orbital frequencies; blue solid line) must be frequency dependent. We demonstrate that the α-β scaling described by Eq. (8) corresponds to a frequency-dependent correction, as it not only modifies the amplitudes but also alters the frequency evolution according to Eq. (17). For comparison, we include the amplitudes as a function of rescaled frequencies (black dashed line) after the application of the α-β scaling. We find visual agreement up to $t_{\rm NR} = -18M$, very close to the merger, between the rescaled ppBHPT amplitudes as a function of rescaled orbital frequencies and NR amplitudes as a function of NR orbital frequencies.

Finally, we generalize the scaling for all modes as

$$h^{\ell,m}_{\rm NR}(\omega_{\rm orb,NR}) \approx \alpha_\ell \times h^{\ell,m}_{\rm ppBHPT}\left(\frac{\omega_{\rm orb,ppBHPT}}{\beta}\right). \quad (17)$$

To further support our observations, we extend our analysis to three additional mass ratio values: $q = [4, 6, 10]$, using

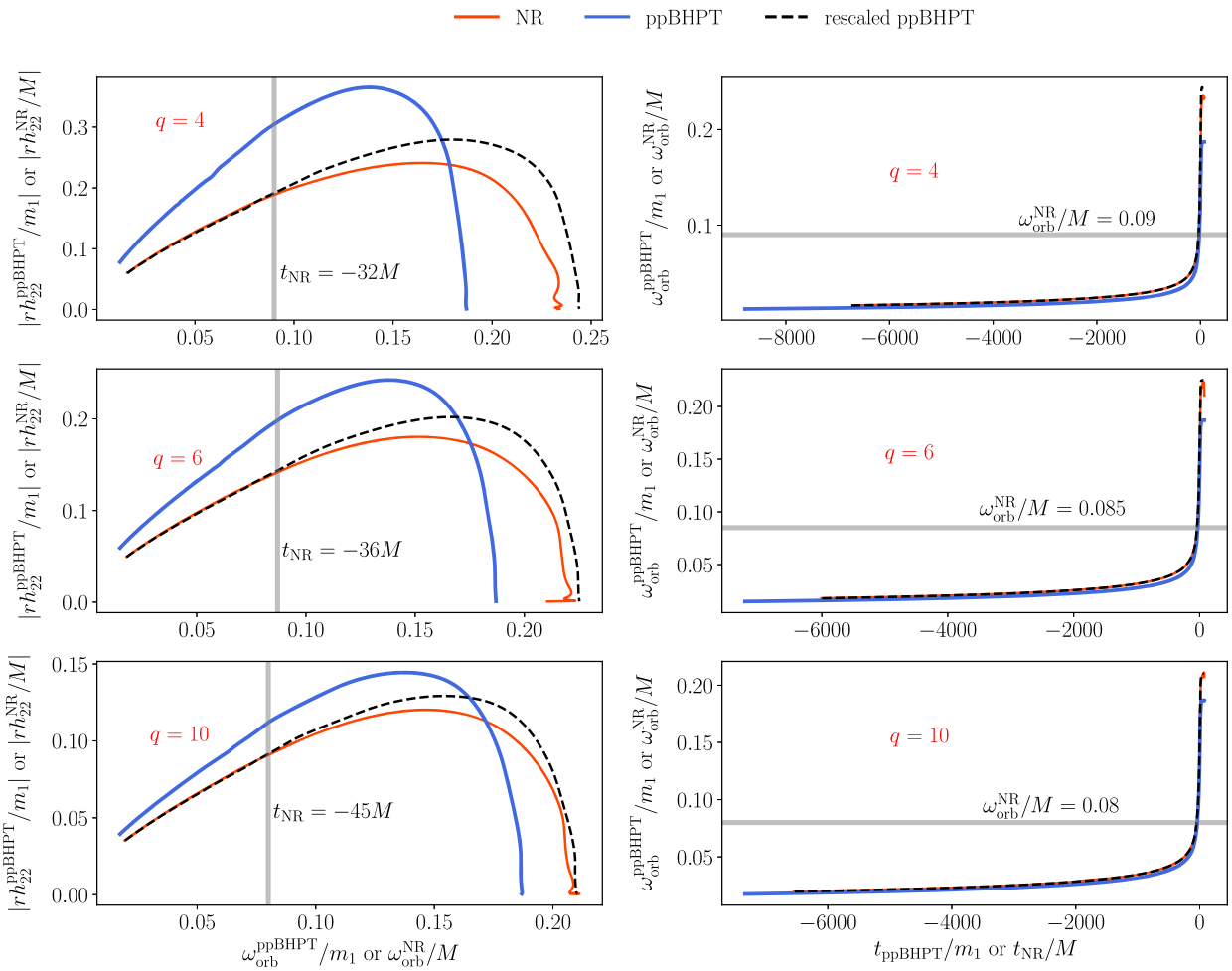

FIG. 7. We show the amplitudes of ppBHPT (red lines) and NR waveforms (blue lines) as a function of orbital frequencies (left panels) for $q = [4, 6, 10]$. Additionally, we include the amplitudes obtained from the approximate scaling given by Eq. (17) (black dashed lines) for comparison. In right panels, we show the orbital frequencies as a function of time. The mass scale of NR and ppBHPT waveforms are M and m_1 respectively. In the left panels, gray vertical lines indicate the time $t_{\rm NR}$ up to which the scaling is effective, while in the right panels, gray horizontal lines represent the orbital frequency $\omega_{\rm orb}$ up to which the scaling holds. Further details can be found in Sec. II D.

publicly available SXS NR data SXS:BBH:1220 [47], SXS:BBH:0181 [48], and SXS:BBH:1107 [49], respectively. However, these NR datasets only cover the final $\sim 6000M$ evolution of the binary, corresponding to approximately 25 orbital cycles. For each mass ratio, we perform the α-β scaling using Eq. (8), obtaining the best-fit values for α and β. We then use Eq. (17) to approximate the rescaled amplitude as a function of the orbital frequency (Fig. 7).

In Fig. 7 (left panels), we compare the amplitudes of both ppBHPT and NR waveforms as a function of the respective orbital frequencies. To gain better understanding, we also plot the orbital frequencies as a function of time in the right panels. During the inspiral phase, the rescaled waveform's amplitude closely matches NR, but deviations become apparent as it approaches the merger. However, the approximate α-β scaling effectively captures the frequency-dependent correction needed to align ppBHPT with NR until very close to the merger, where the scaling breaks down. Specifically, we find that the scaling remains effective up to $t_{\rm NR} = -32M$ for $q = 4$, $t_{\rm NR} = -36M$ for $q = 6$, and $t_{\rm NR} = -45M$ for $q = 10$. This suggests that the α-β scaling successfully matches NR data very well up to the plunge phase.

It is worth mentioning that the reason for the global α-β fit to be less effective around merger is that the global-fit values deviate from the local optimal α-β estimates in this regime (Fig. 3). These deviations can also be attributed to the changes in mass and spin of the final black hole during this phase [43]. Incorporating the updated final mass and spin values in the ppBHPT framework is expected to reduce these deviations and improve the accuracy of the rescaling [43].

III. COMPARISON AGAINST POST-NEWTONIAN THEORY

We now provide a detailed comparison of the post-Newtonian theory waveforms with ppBHPT, rescaled ppBHPT (obtained through the α-β procedure), and NR in the comparable mass regime. A detailed review of post-Newtonian methods are given in Ref. [34]. The post-Newtonian approximation is a slow-motion, weak-field approximation to general relativity with an expansion parameter $\xi = \frac{v}{c}$ where v is the magnitude of the relative velocity and c is the speed of light. While many previous analysis have focused on understanding the match between NR and PN in the comparable mass regime [50–53], our focus remains in comparing ppBHPT to PN.

A. Comparing waveforms at $q = 3$

We show the full (2, 2) mode inspiral-merger-ringdown waveforms from NR (blue solid lines), rescaled ppBHPT (black dashed lines), and PN (green dash-dotted lines) in Fig. 8. In particular, we use TaylorT4 PN approximation, generated using LALSimulation software package. This

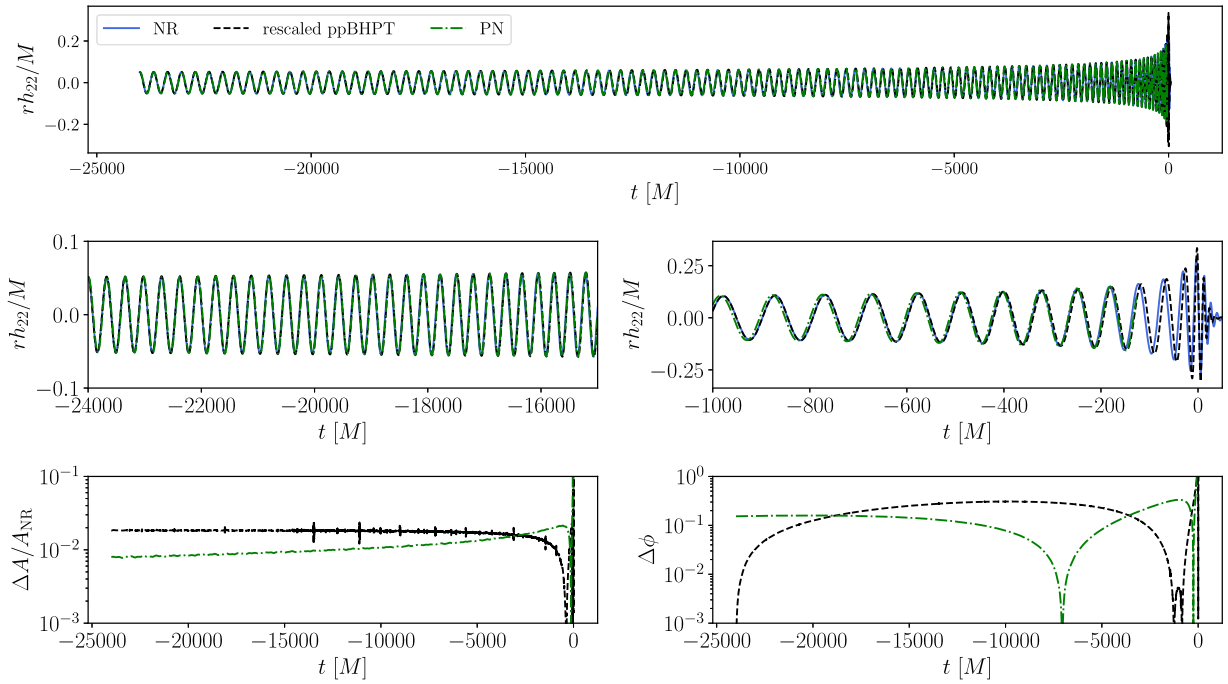

FIG. 8. We show the waveforms for the full (2, 2) mode inspiral-merger-ringdown from NR (blue solid lines), rescaled ppBHPT (black dashed lines), and PN (green dash-dotted lines) for $q = 3$. All waveforms have the mass scale of M. The upper panel displays the waveforms for the entire duration, while the second row focuses on the early inspiral and the merger-ringdown phases. In the third row of the figure, we provide the errors in both the rescaled ppBHPT and PN waveforms when compared to NR. Further details can be found in Sec. III.

particular approximation includes phase terms up to 3.5PN order and amplitude terms up to 2.5PN order [50]. We zoom into the earlier and later times of the waveform to examine the match between rescaled ppBHPT, PN, and NR in more detail. Additionally, we compute the relative error in the amplitude and the absolute phase error for both rescaled ppBHPT and PN compared to NR. The results indicate that both rescaled ppBHPT and PN exhibit similar errors in the amplitude when compared to NR. However, in the late inspiral phase (e.g., $-4000M \leq t \leq -100M$), the rescaled ppBHPT waveform yields a much smaller error in the phase compared to the PN waveform. This suggests that the rescaled ppBHPT waveform provides improved accuracy in capturing the phase evolution of the system during the late-inspiral regime, as compared to the PN approximation. This is expected as, in the late inspiral, the binary moves into the strong field and the PN approximation breaks down.

Finally, in Fig. 9, we present the amplitude of the ppBHPT, rescaled ppBHPT, NR, and PN waveforms as a function of the respective orbital frequencies. The amplitude evolution extracted from NR is compared to both the PN and rescaled ppBHPT waveforms. We observe that in the inspiral region, both the PN and rescaled ppBHPT amplitudes agree well with the amplitude evolution obtained from NR. However, as we progress towards later times, the PN approximation starts deviating from NR around $t_{\rm NR} = -708M$, while the rescaled ppBHPT approximation breaks down around $t_{\rm NR} = -18M$. This suggests that the rescaled ppBHPT waveform better captures the dynamics of NR compared to the PN waveform.

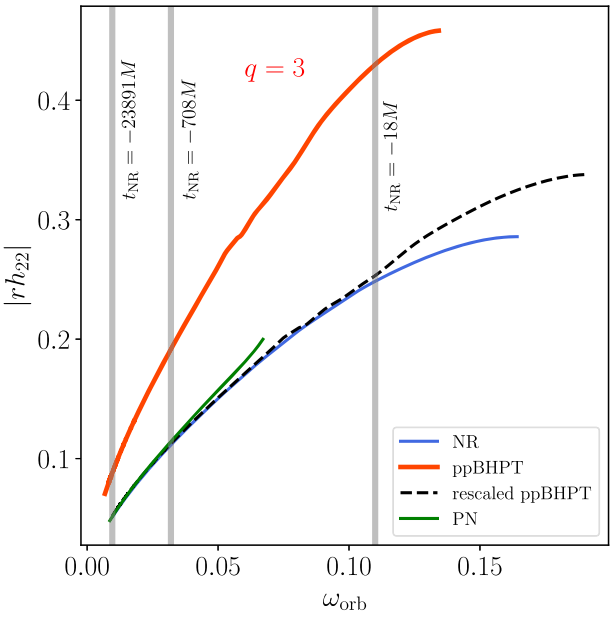

FIG. 9. We show the amplitudes of ppBHPT (red lines), NR waveforms (blue lines) and PN (green lines) as a function of orbital frequencies for $q = 3$. Additionally, we include the amplitudes obtained from the approximate scaling given by Eq. (17) (black dashed lines) for comparison. The mass scale of NR and ppBHPT waveforms are M and m_1 respectively. Gray vertical lines indicate the time $t_{\rm NR}$ up to which PN and α-β rescaling shows remarkable match with NR. More details are in Sec. III.

B. Estimating α-β using PN

Our analysis in Secs. II B, II C, and III A highlights interesting possibilities for using PN waveforms to accurately estimate global values for α and β. We are motivated by the following observations:

(i) The values of α and β remain nearly constant for a significant duration of the binary evolution, with only slight deviations around the merger. These local estimates of α and β closely align with the values obtained using global-error minimization techniques. Furthermore, the values of α and β obtained using only the inspiral part of the waveform exhibit remarkable agreement with the values obtained using the full waveform data.

(ii) While the PN approximation breaks down towards the merger (e.g., at $t = -708M$ in Fig. 9, or about 11 cycles before merger as reported in Ref. [53]), it provides an excellent match to NR waveforms in the inspiral phase, which is far away from the merger.

These observations suggest that PN waveforms can be used to infer the α and β values required to match a ppBHPT waveform to PN. These α and β values will be very close to the values obtained using NR data. This procedure has significant implications. Firstly, it means that one can use ppBHPT and PN waveforms in the early inspiral to obtain the α-β values and generate a rescaled ppBHPT waveform that matches NR waveforms throughout the entire binary evolution, from inspiral to ringdown.

In this section, we investigate the possibility of using PN waveforms for estimating α and β in great detail using different PN approximations.

1. α-β PN scaling at $q = 3$

First, we perform a calibration between the ppBHPT waveform at $q = 3$ and a PN waveform generated using the `TaylorT4` approximation. We obtain $\alpha_{\rm PN}$ and $\beta_{\rm PN}$ as the calibration parameters. Interestingly, we find that these values are very close to $\alpha_{\rm NR,ins}$ and $\beta_{\rm iNR,ins}$ obtained by comparing the inspiral portion of the NR and ppBHPT waveforms, as well as $\alpha_{\rm NR,full}$ and $\beta_{\rm NR,full}$ obtained from the comparison of full NR and ppBHPT waveforms. Specifically, we have

$$[\alpha_{\rm PN}, \beta_{\rm PN}] = [0.738862, 0.705607],$$
$$[\alpha_{\rm NR,full}, \beta_{\rm NR,full}] = [0.737122, 0.706900],$$
$$[\alpha_{\rm NR,ins}, \beta_{\rm iNR,ins}] = [0.731040, 0.707100].$$

Furthermore, we utilize $\alpha_{\rm PN}$ and $\beta_{\rm PN}$ to rescale the ppBHPT waveform, and we observe an excellent match with the NR

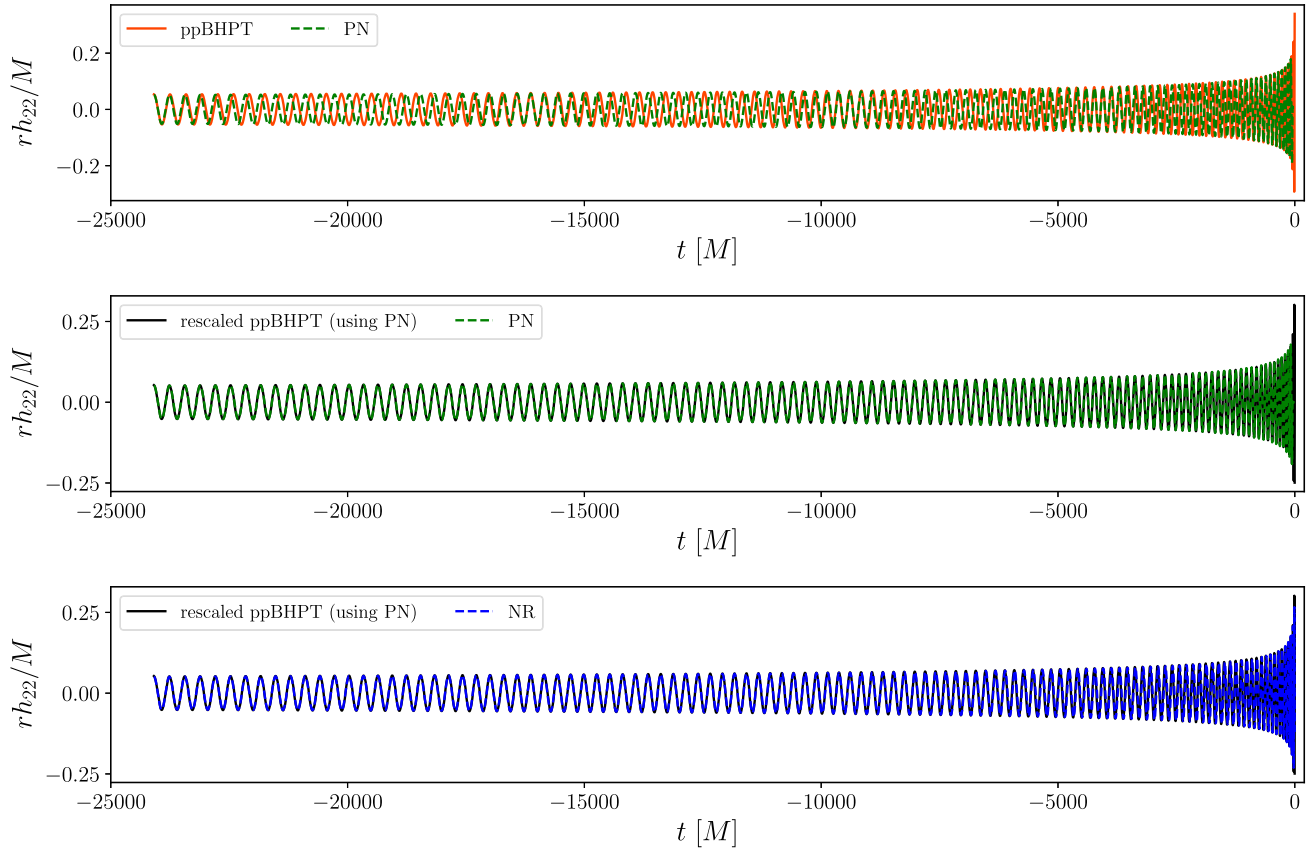

FIG. 10. We show the comparison of the (2, 2) mode of the PN and ppBHPT waveforms (first row), along with the comparison between PN and rescaled ppBHPT waveforms (second row) for $q = 3$. Rescaled ppBHPT waveform is obtained by performing an α-β calibration to PN. For comparison, we also show the NR waveform in the third row. All waveforms have the mass-scale of M. More details are in Sec. III B.

data not only in the inspiral phase (Fig. 10, third row). We however notice some dephasing in the merger-ringdown part. Nonetheless, this analysis suggests that PN waveforms, which mostly capture the inspiral phase, can provide meaningful estimates of α and β for rescaling ppBHPT waveforms to match NR waveforms reasonably well in the inspiral part. For example, the L_2-norm error between ppBHPT and NR waveform up to merger in Fig. 10 is ∼0.9. However, the L_2-norm error between PN and NR in that time window is ∼0.02 whereas the error between PN-rescaled ppBHPT and NR is ∼0.06. Once we obtain the scaled ppBHPT waveforms for the inspiral, we can then utilize the framework developed in Ref. [43] to obtain appropriately scaled ppBHPT waveform at the merger-ringdown part too.

2. α-β PN scaling at $q = [4, 6, 10]$

To investigate the validity of our observations for different mass ratios, we repeat the analysis for mass ratios $q = 4$, $q = 6$, and $q = 10$. In Fig. 11, we present the values of α and β obtained by rescaling the ppBHPT waveforms to both NR and PN data. We find that $\beta_{\rm PN}$, obtained from the PN waveform, closely matches $\beta_{\rm NR}$ for all mass ratios. This suggests that the β parameter is relatively insensitive to the choice of waveform and is consistent between NR and PN. However, we observe that $\alpha_{\rm PN}$, also obtained from the PN waveform, is systematically larger than the values obtained from NR. This difference appears to increase as the mass ratio increases. Nevertheless, it is noteworthy that the values of α obtained from PN are still quite close to those obtained from NR, indicating a reasonable agreement between the two.

3. Understanding the effect of the choice of PN model

It is important to note that each PN model includes corrections up to a certain PN order, and these higher-order corrections can affect the accuracy of the rescaling. To investigate the effect of different PN models on the α-β calibration, we repeat the calibration process for $q = 3$ using different PN approximations: `TaylorT1`, `TaylorT2`, and `TaylorT4`. While all of these approximation includes phase terms up to 3.5PN order and amplitude terms up to 2.5PN order, they employ different techniques and expansions to obtain these terms [54,55]. This allows us to assess whether the choice of PN model

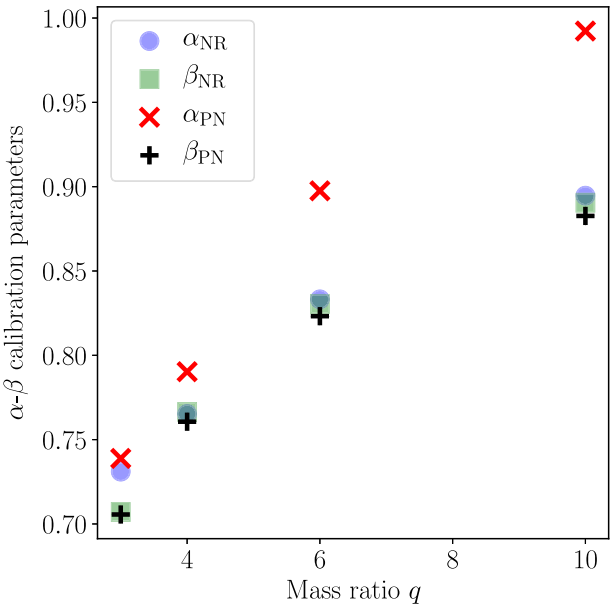

FIG. 11. We show the α and β values for a set of mass ratios obtained by performing the calibration against NR and PN waveforms. For PN, we use only the inspiral data to obtain the values of α and β whereas full IMR waveform is used for NR. More details are in Sec. III B 2.

affects the resulting values of α and β. By performing the α-β calibration with different PN approximations, we obtain slightly different values for α and β. In particular, we find,

$$\left[\alpha_{\rm PN}^{\rm TaylorT4}, \beta_{\rm PN}^{\rm TaylorT4}\right] = [0.738862, 0.705607],$$
$$\left[\alpha_{\rm PN}^{\rm TaylorT1}, \beta_{\rm PN}^{\rm TaylorT1}\right] = [0.745278, 0.709454],$$
$$\left[\alpha_{\rm PN}^{\rm TaylorT2}, \beta_{\rm PN}^{\rm TaylorT2}\right] = [0.753860, 0.709265].$$

It is interesting to note that value of β changes marginally when we use a different PN model. However, changes in α is more prominent. This indicates that the choice of PN model does have a slight an impact on the rescaling parameters.

IV. DISCUSSION AND CONCLUSION

In this paper, we investigated the validity and effectiveness of the α-β scaling approach, previously introduced by Islam *et al.* [36], which aims to match the ppBHPT waveforms to the NR waveforms. Utilizing publicly available long NR data (`SXS:BBH:2265`) for mass ratio $q = 3$, we demonstrated that the scaling can be achieved even for longer NR simulations, spanning up to $\sim 30000M$ in duration. Throughout most of the binary evolution, the scaling factors α and β can be computed utilizing publicly available long NR data (`SXS:BBH:2265`) for mass ratio $q = 3$ and considered approximately constant, although they show slight deviations close to the merger. These deviations are expected due to the loss of energy and change in mass and spin of the final black hole during the merger process. Once the final mass and spin values are incorporated into the ppBHPT framework, these deviations are expected to be reduced [43].

Furthermore, we investigated the frequency-dependent nature of the scaling. We derived the α-β scaling as a function of orbital frequencies and demonstrated its equivalence to a frequency-dependent correction. The rescaled ppBHPT waveform, when matched to NR amplitudes as a function of orbital frequencies, showed excellent agreement, providing further support for the frequency-dependent nature of the scaling.

We then compared the accuracy of the rescaled ppBHPT waveform obtained through the α-β scaling against the `TaylorT4` PN approximation. The rescaled ppBHPT waveform showed comparable accuracy to the PN waveform in terms of amplitude, but exhibited significantly smaller phase errors during the late inspiral phase. Our analysis confirms the feasibility of using PN waveforms to derive precise α-β calibration parameters. The calibration process involves matching the ppBHPT waveform to a PN waveform, focusing on the inspiral phase. The resulting α and β values obtained from this calibration closely align with those obtained from NR waveforms.

Overall, our results demonstrate that the α-β scaling provides an effective method for matching ppBHPT waveforms to NR waveforms in the comparable mass regime, accounting for missing finite-size effects and possibly higher-order self-force corrections [42,44]. The scaling is frequency dependent, capturing the correct amplitude and frequency evolution of the NR waveforms. While the scaling has limitations close to the merger (due to a change in mass and spin values [43]), it remains highly effective in reproducing NR dynamics up to the plunge phase. These findings have implications for gravitational wave observations and waveform modeling in extreme-mass-ratio inspirals.

ACKNOWLEDGMENTS

We thank Scott Field, Scott Hughes, Adam Pound, Niels Warburton, Barry Wardell, and Chandra Kant Mishra for helpful discussions and thoughtful comments on the manuscript. The authors acknowledge support of NSF Grants No. PHY-2106755, No. PHY-2307236 (G. K.), No. DMS-1912716, and No. DMS-2309609 (T. I. and G. K.). Simulations were performed on CARNiE at the Center for Scientific Computing and Visualization Research (CSCVR) of UMassD, which is supported by the Office of Naval Research (ONR)/Defense University Research Instrumentation Program (DURIP) Grant No. N00014181255 and the UMass-URI UNITY supercomputer supported by the Massachusetts Green High Performance Computing Center (MGHPCC).

[1] Jonathan Blackman, Scott E. Field, Chad R. Galley, Béla Szilágyi, Mark A. Scheel, Manuel Tiglio, and Daniel A. Hemberger, Fast and accurate prediction of numerical relativity waveforms from binary black hole coalescences using surrogate models, Phys. Rev. Lett. **115**, 121102 (2015).

[2] Jonathan Blackman, Scott E. Field, Mark A. Scheel, Chad R. Galley, Christian D. Ott, Michael Boyle, Lawrence E. Kidder, Harald P. Pfeiffer, and Béla Szilágyi, Numerical relativity waveform surrogate model for generically precessing binary black hole mergers, Phys. Rev. D **96**, 024058 (2017).

[3] Jonathan Blackman, Scott E. Field, Mark A. Scheel, Chad R. Galley, Daniel A. Hemberger, Patricia Schmidt, and Rory Smith, A surrogate model of gravitational waveforms from numerical relativity simulations of precessing binary black hole mergers, Phys. Rev. D **95**, 104023 (2017).

[4] Vijay Varma, Scott E. Field, Mark A. Scheel, Jonathan Blackman, Lawrence E. Kidder, and Harald P. Pfeiffer, Surrogate model of hybridized numerical relativity binary black hole waveforms, Phys. Rev. D **99**, 064045 (2019).

[5] Vijay Varma, Scott E. Field, Mark A. Scheel, Jonathan Blackman, Davide Gerosa, Leo C. Stein, Lawrence E. Kidder, and Harald P. Pfeiffer, Surrogate models for precessing binary black hole simulations with unequal masses, Phys. Rev. Res. **1**, 033015 (2019).

[6] Tousif Islam, Vijay Varma, Jackie Lodman, Scott E. Field, Gaurav Khanna, Mark A. Scheel, Harald P. Pfeiffer, Davide Gerosa, and Lawrence E. Kidder, Eccentric binary black hole surrogate models for the gravitational waveform and remnant properties: Comparable mass, nonspinning case, Phys. Rev. D **103**, 064022 (2021).

[7] Alejandro Bohé *et al.*, Improved effective-one-body model of spinning, nonprecessing binary black holes for the era of gravitational-wave astrophysics with advanced detectors, Phys. Rev. D **95**, 044028 (2017).

[8] Roberto Cotesta, Alessandra Buonanno, Alejandro Bohé, Andrea Taracchini, Ian Hinder, and Serguei Ossokine, Enriching the symphony of gravitational waves from binary black holes by tuning higher harmonics, Phys. Rev. D **98**, 084028 (2018).

[9] Roberto Cotesta, Sylvain Marsat, and Michael Pürrer, Frequency domain reduced order model of aligned-spin effective-one-body waveforms with higher-order modes, Phys. Rev. D **101**, 124040 (2020).

[10] Yi Pan, Alessandra Buonanno, Andrea Taracchini, Lawrence E. Kidder, Abdul H. Mroué, Harald P. Pfeiffer, Mark A. Scheel, and Béla Szilágyi, Inspiral-merger-ringdown waveforms of spinning, precessing black-hole binaries in the effective-one-body formalism, Phys. Rev. D **89**, 084006 (2014).

[11] Stanislav Babak, Andrea Taracchini, and Alessandra Buonanno, Validating the effective-one-body model of spinning, precessing binary black holes against numerical relativity, Phys. Rev. D **95**, 024010 (2017).

[12] Sascha Husa, Sebastian Khan, Mark Hannam, Michael Pürrer, Frank Ohme, Xisco Jiménez Forteza, and Alejandro Bohé, Frequency-domain gravitational waves from nonprecessing black-hole binaries. I. New numerical waveforms and anatomy of the signal, Phys. Rev. D **93**, 044006 (2016).

[13] Sebastian Khan, Sascha Husa, Mark Hannam, Frank Ohme, Michael Pürrer, Xisco Jiménez Forteza, and Alejandro Bohé, Frequency-domain gravitational waves from nonprecessing black-hole binaries. II. A phenomenological model for the advanced detector era, Phys. Rev. D **93**, 044007 (2016).

[14] Lionel London, Sebastian Khan, Edward Fauchon-Jones, Cecilio García, Mark Hannam, Sascha Husa, Xisco Jiménez-Forteza, Chinmay Kalaghatgi, Frank Ohme, and Francesco Pannarale, First higher-multipole model of gravitational waves from spinning and coalescing black-hole binaries, Phys. Rev. Lett. **120**, 161102 (2018).

[15] Sebastian Khan, Katerina Chatziioannou, Mark Hannam, and Frank Ohme, Phenomenological model for the gravitational-wave signal from precessing binary black holes with two-spin effects, Phys. Rev. D **100**, 024059 (2019).

[16] Abdul H. Mroue *et al.*, Catalog of 174 binary black hole simulations for gravitational wave astronomy, Phys. Rev. Lett. **111**, 241104 (2013).

[17] Michael Boyle *et al.*, The SXS Collaboration catalog of binary black hole simulations, Classical Quantum Gravity **36**, 195006 (2019).

[18] James Healy, Carlos O. Lousto, Yosef Zlochower, and Manuela Campanelli, The RIT binary black hole simulations catalog, Classical Quantum Gravity **34**, 224001 (2017).

[19] James Healy, Carlos O. Lousto, Jacob Lange, Richard O'Shaughnessy, Yosef Zlochower, and Manuela Campanelli, Second RIT binary black hole simulations catalog and its application to gravitational waves parameter estimation, Phys. Rev. D **100**, 024021 (2019).

[20] James Healy and Carlos O. Lousto, Third RIT binary black hole simulations catalog, Phys. Rev. D **102**, 104018 (2020).

[21] James Healy and Carlos O. Lousto, Fourth RIT binary black hole simulations catalog: Extension to eccentric orbits, Phys. Rev. D **105**, 124010 (2022).

[22] Karan Jani, James Healy, James A. Clark, Lionel London, Pablo Laguna, and Deirdre Shoemaker, Georgia Tech catalog of gravitational waveforms, Classical Quantum Gravity **33**, 204001 (2016).

[23] Eleanor Hamilton *et al.*, A catalogue of precessing black-hole-binary numerical-relativity simulations, arXiv:2303.05419.

[24] Pranesh A. Sundararajan, Gaurav Khanna, and Scott A. Hughes, Towards adiabatic waveforms for inspiral into Kerr black holes. I. A New model of the source for the time domain perturbation equation, Phys. Rev. D **76**, 104005 (2007).

[25] Pranesh A. Sundararajan, Gaurav Khanna, Scott A. Hughes, and Steve Drasco, Towards adiabatic waveforms for inspiral into Kerr black holes: II. Dynamical sources and generic orbits, Phys. Rev. D **78**, 024022 (2008).

[26] Pranesh A. Sundararajan, Gaurav Khanna, and Scott A. Hughes, Binary black hole merger gravitational waves and recoil in the large mass ratio limit, Phys. Rev. D **81**, 104009 (2010).

[27] Anil Zenginoglu and Gaurav Khanna, Null infinity waveforms from extreme-mass-ratio inspirals in Kerr spacetime, Phys. Rev. X **1**, 021017 (2011).

[28] Ryuichi Fujita and Hideyuki Tagoshi, New numerical methods to evaluate homogeneous solutions of the Teukolsky equation, Prog. Theor. Phys. **112**, 415 (2004).

[29] Ryuichi Fujita and Hideyuki Tagoshi, New numerical methods to evaluate homogeneous solutions of the Teukolsky equation II. Solutions of the continued fraction equation, Prog. Theor. Phys. **113**, 1165 (2005).
[30] Shuhei Mano, Hisao Suzuki, and Eiichi Takasugi, Analytic solutions of the Teukolsky equation and their low frequency expansions, Prog. Theor. Phys. **95**, 1079 (1996).
[31] William William Thomas Throwe, High precision calculation of generic extreme mass ratio inspirals, Ph.D. thesis, Massachusetts Institute of Technology, 2010.
[32] Stephen O'Sullivan and Scott A. Hughes, Strong-field tidal distortions of rotating black holes: Formalism and results for circular, equatorial orbits, Phys. Rev. D **90**, 124039 (2014); **91**, 109901(E) (2015).
[33] Steve Drasco and Scott A. Hughes, Gravitational wave snapshots of generic extreme mass ratio inspirals, Phys. Rev. D **73**, 024027 (2006); **88**, 109905(E) (2013); **90**, 109905(E) (2014).
[34] Luc Blanchet, Gravitational radiation from post-Newtonian sources and inspiralling compact binaries, Living Rev. Relativity **17**, 2 (2014).
[35] Nur E. M. Rifat, Scott E. Field, Gaurav Khanna, and Vijay Varma, Surrogate model for gravitational wave signals from comparable and large-mass-ratio black hole binaries, Phys. Rev. D **101**, 081502 (2020).
[36] Tousif Islam, Scott E. Field, Scott A. Hughes, Gaurav Khanna, Vijay Varma, Matthew Giesler, Mark A. Scheel, Lawrence E. Kidder, and Harald P. Pfeiffer, Surrogate model for gravitational wave signals from nonspinning, comparable-to large-mass-ratio black hole binaries built on black hole perturbation theory waveforms calibrated to numerical relativity, Phys. Rev. D **106**, 104025 (2022).
[37] Barry Wardell, Adam Pound, Niels Warburton, Jeremy Miller, Leanne Durkan, and Alexandre Le Tiec, Gravitational waveforms for compact binaries from second-order self-force theory, Phys. Rev. Lett. **130**, 241402 (2023).
[38] Carlos O. Lousto and James Healy, Exploring the small mass ratio binary black hole merger via Zeno's dichotomy approach, Phys. Rev. Lett. **125**, 191102 (2020).
[39] Carlos O. Lousto and James Healy, Study of the intermediate mass ratio black hole binary merger up to 1000:1 with numerical relativity, Classical Quantum Gravity **40**, 09LT01 (2023).
[40] Jooheon Yoo, Vijay Varma, Matthew Giesler, Mark A. Scheel, Carl-Johan Haster, Harald P. Pfeiffer, Lawrence E. Kidder, and Michael Boyle, Targeted large mass ratio numerical relativity surrogate waveform model for GW190814, Phys. Rev. D **106**, 044001 (2022).
[41] Matthew Giesler, Mark A. Scheel, and Saul A. Teukolsky, Numerical simulations of extreme mass ratio binary black holes (to be published).
[42] Tousif Islam, Interplay between numerical relativity and black hole perturbation theory in the intermediate-mass-ratio regime, Phys. Rev. D **108**, 044013 (2023).
[43] Tousif Islam, Scott E. Field, and Gaurav Khanna, Remnant black hole properties from numerical-relativity-informed perturbation theory and implications for waveform modelling, Phys. Rev. D **108**, 064048 (2023).
[44] Tousif Islam and Gaurav Khanna, Interplay between numerical relativity and perturbation theory: Finite size effects, Phys. Rev. D **108**, 044012 (2023).
[45] SXS Collaboration, Binary black-hole simulation `SXS:BBH:2265`, 10.5281/zenodo.3387428 (2019).
[46] S. E. Field, S. Gottlieb, Z. J. Grant, L. F. Isherwood, and G. Khanna, A GPU-accelerated mixed-precision WENO method for extremal black hole and gravitational wave physics computations, Commun. Appl. Math. Comput. Sci. **5**, 97 (2023).
[47] Jonathan Blackman (SXS Collaboration), Binary black-hole simulation `SXS:BBH:1220` (2019), 10.5281/zenodo.3302203.
[48] Jonathan Blackman, Larry Kidder, Harald Pfeiffer, Mark Scheel, Michael Boyle, Dan Hemberger, Geoffrey Lovelace, and Bela Szilagyi, Binary black-hole simulation `SXS:BBH:0181`, 10.5281/zenodo.3302087 (2019).
[49] SXS Collaboration, Binary black-hole simulation `SXS:BBH:1107`, 10.5281/zenodo.3302023 (2019).
[50] Michael Boyle, Duncan A. Brown, Lawrence E. Kidder, Abdul H. Mroue, Harald P. Pfeiffer, Mark A. Scheel, Gregory B. Cook, and Saul A. Teukolsky, High-accuracy comparison of numerical relativity simulations with post-Newtonian expansions, Phys. Rev. D **76**, 124038 (2007).
[51] Mark Hannam, Sascha Husa, Bernd Bruegmann, and Achamveedu Gopakumar, Comparison between numerical-relativity and post-Newtonian waveforms from spinning binaries: The orbital hang-up case, Phys. Rev. D **78**, 104007 (2008).
[52] Yi Pan, Alessandra Buonanno, John G. Baker, Joan Centrella, Bernard J. Kelly, Sean T. McWilliams, Frans Pretorius, and James R. van Meter, A data-analysis driven comparison of analytic and numerical coalescing binary waveforms: Nonspinning case, Phys. Rev. D **77**, 024014 (2008).
[53] Mark Hannam, Sascha Husa, Ulrich Sperhake, Bernd Bruegmann, and Jose A. Gonzalez, Where post-Newtonian and numerical-relativity waveforms meet, Phys. Rev. D **77**, 044020 (2008).
[54] Thibault Damour, Bala R. Iyer, and B. S. Sathyaprakash, A comparison of search templates for gravitational waves from binary inspiral, Phys. Rev. D **63**, 044023 (2001); **72**, 029902(E) (2005).
[55] Thibault Damour, Bala R. Iyer, and B. S. Sathyaprakash, A comparison of search templates for gravitational waves from binary inspiral—3.5PN update, Phys. Rev. D **66**, 027502 (2002).